





Cite this: *RSC Adv.*, 2024, 14, 16349

Design, synthesis, and anti-inflammatory activity of indole-2-formamide benzimidazole[2,1-*b*]thiazole derivatives†

Hai-Feng Lin, ^a Yu-Cai Jiang, ^{*b} Zhi-Wei Chen ^c and Lin-Lin Zheng^d

Molecular hybridization is a widely employed technique in medicinal chemistry for drug modification, aiming to enhance pharmacological activity and minimize side effects. The combination of an indole ring and imidazole[2,1-*b*]thiazole has shown promising potential as a group that exhibits potent anti-inflammatory effects. In this study, we designed and synthesized a series of derivatives comprising indole-2-formamide benzimidazole[2,1-*b*]thiazole to evaluate their impact on LPS-induced production of pro-inflammatory cytokines NO, IL-6, and TNF- α release, as well as iron death in RAW264.7 cells. The findings revealed that most compounds effectively inhibited LPS-induced production of pro-inflammatory cytokines NO, IL-6, and TNF- α release in RAW264.7 cells. Compound **13b** exhibited the most potent anti-inflammatory activity among the tested compounds. The results of the cytotoxicity assay indicated that compound **13b** was nontoxic. Additionally, compound **13b** was found to elevate the levels of ROS, MDA, and Fe²⁺, while reducing GSH content, thereby facilitating the iron death process. Consequently, compound **13b** showed promise for future development as an anti-inflammatory drug.

Received 22nd January 2024

Accepted 30th April 2024

DOI: 10.1039/d4ra00557k

rsc.li/rsc-advances

Introduction

Inflammation is the natural immune response of the body to pathogens, physical injuries, and irritants, and is characterized by localized symptoms such as redness, swelling, heat, and pain, as well as systemic effects including fever, chills, and organ dysfunction.¹ Clinical manifestations vary among individuals, with inflammation typically serving as a protective response to dilute toxins, remove inflammatory agents, and prevent the spread of microorganisms throughout various bodily systems. Additionally, inflammation aids in the regeneration of tissues and organs.² Pro-inflammatory mediators, including nitrogen monoxide (NO), interleukin-6 (IL-6), tumor necrosis factor- α (TNF- α), and interleukin-1 β (IL-1 β), are essential for facilitating tissue and cell healing as well as for the prevention and management of a number of illnesses.^{3–5} However, excessive production of pro-inflammatory mediators or their inadequate control may lead to acute lung damage, rheumatoid arthritis, and chronic inflammatory conditions in

the gut.^{6,7} Therefore, it is crucial to identify highly effective medications and treatments that efficiently inhibit the synthesis and release of these cytokines.

The fusion of numerous heterocyclic compounds, including nitrogen and sulfur atoms, plays an essential role in the field of medicinal chemistry.^{8,9} These chemicals are extensively used to treat a broad range of conditions. Indole and imidazole[2,1-*b*]thiazole derivatives have garnered considerable interest, probably owing to their extensive pharmacological activities. These activities include anti-tumor effects,^{10,11} antibacterial properties,^{12,13} anti-inflammatory and analgesic effects,^{14,15} as well as antioxidant capabilities.^{16,17} Importantly, indomethacin **1**, compound **2**,¹⁸ compound **3**,¹⁹ compound **4**,¹⁵ compound **5**,²⁰ and compound **6**²⁰ have shown favorable anti-inflammatory activities and safety (Fig. 1).

Molecular hybridization is widely used in pharmaceutical chemistry, involving the combination of two drug molecules or their pharmacodynamic groups into a single entity.²¹ This strategy leads to produce new chemicals with combined features of the original medications that demonstrate synergistic therapy benefits or reduce adverse effects.²² The non-steroidal anti-inflammatory medicine benorylate is a notable example of a hybrid molecule, produced by combining the carboxyl group of aspirin with the phenolic hydroxyl group of acetaminophen. This combination results in the formation of a hybrid molecule adjusted to reduce the incidence of gastrointestinal discomfort.

Based on results of previous studies, this research group devised and synthesized a series of indole-2-formamide

^aDepartment of Gastroenterology, Affiliated Hospital of Putian University, Putian, China

^bDepartment of Pharmacy, Affiliated Hospital of Putian University, Putian, China. E-mail: jiangyucai2030@ptu.edu.cn

^cDepartment of Pathology, Affiliated Hospital of Putian University, Putian, China

^dDepartment of Oncology, Affiliated Hospital of Putian University, Putian, China

† Electronic supplementary information (ESI) available: Synthetic procedure and its characterization ¹H NMR, ¹³C NMR, HR-MS data of target compounds. See DOI: <https://doi.org/10.1039/d4ra00557k>

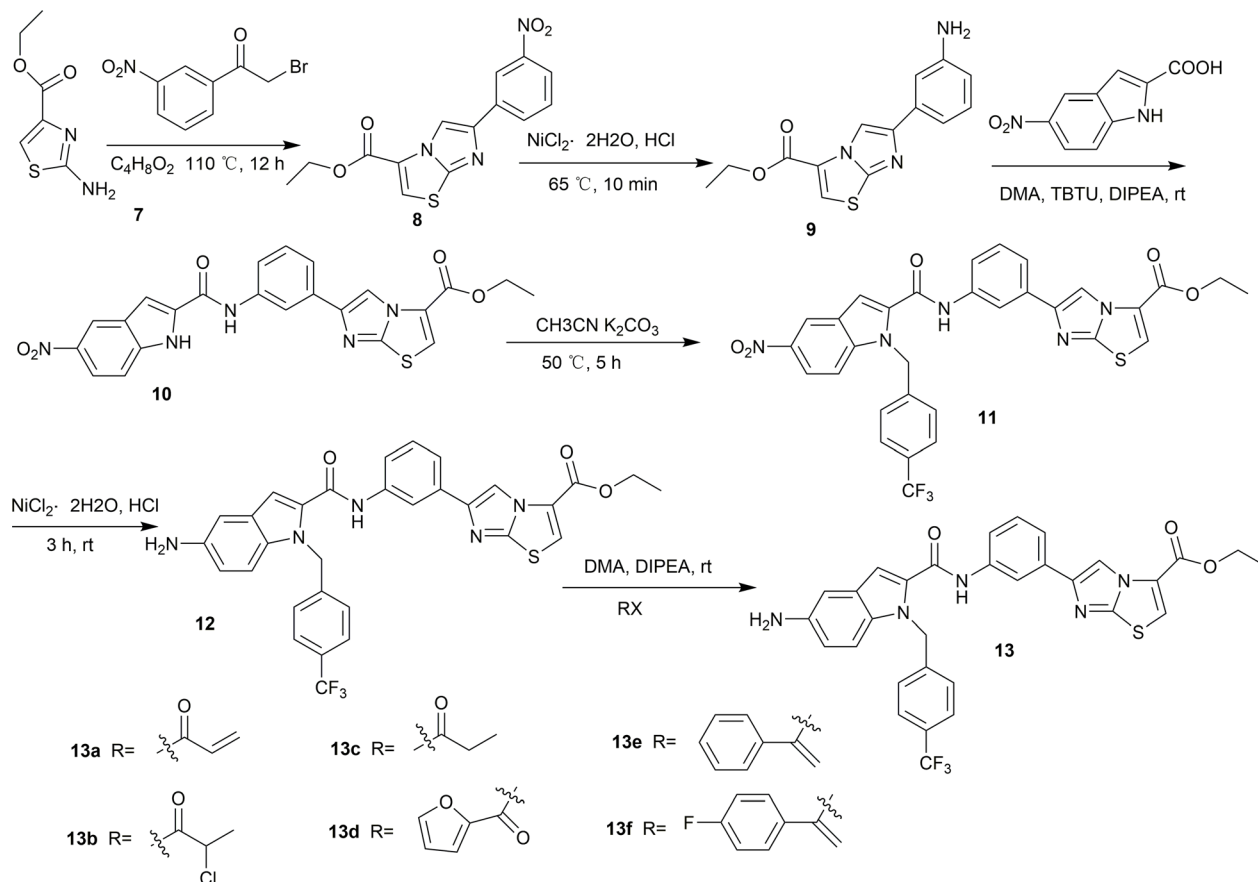



was accomplished by using tin(II) chloride dihydrate and strong hydrochloric acid. Additionally, the use of DIPEA as a catalyst allowed for effective completion of reactions between nucleophile **12** and various acyl halides in DMA. These reactions led to the synthesis of compounds **13a–13f** of the compound series. Proton nuclear magnetic resonance (^1H NMR), carbon nuclear magnetic resonance (^{13}C NMR), and high-resolution electrospray ionization mass spectrometry (HR-ESI-MS) were used to comprehensively characterize the newly synthesized indole-2-formamide benzimidazole[2,1-*b*]thiazole derivatives.

Chemistry

Initial evaluation against LPS-induced NO, IL-6, and TNF- α release by the derivatives (13a-13f)

In terms of the progression of the systemic inflammatory response, LPS has a significant role, notably in the synthesis of proinflammatory cytokines such as NO, IL-6, and TNF- α . To determine whether the compounds possessed anti-inflammatory effects (Fig. 2), an evaluation was conducted using the Griess reagent test to determine the inhibitory effects of the synthesized compounds on the production of NO by LPS in RAW264.7 cells. Additionally, the enzyme-linked immunosorbent assay (ELISA) was utilized to assess the inhibitory effects of these compounds on the production of IL-6 and TNF- α by LPS in RAW264.7 cells. A demonstration of the inhibitory effects of the derivatives on the release of NO, IL-6, and TNF- α from RAW264.7 cells that have been stimulated by LPS can be discovered in Fig. 2. The vast majority of the compounds exhibited varying degrees of inhibition in LPS-activated RAW264.7 cells. Furthermore, these effects increased as the dose of the drug increased, particularly with respect to NO and IL-6 levels.



Scheme 1 Synthetic routes of indole-2-formamide benzimidazole[2,1-*b*]thiazole derivatives (13a–13f).

Dose-dependent inhibition of NO, IL-6, and TNF- α release by the derivatives (13a, 13b, and 13d–13f)

The compounds capable of inhibiting the release of NO, IL-6, and TNF- α were selected based on their anti-inflammatory activity, and subsequent the half maximal inhibitory concentration (IC₅₀) assays were conducted with dose-response experiments. According to the anti-inflammatory activity, compounds that can inhibit the release of NO, IL-6, and TNF- α were screened. Compounds **13a**, **13b**, and **13d–13f** were selected for subsequent experiments. As shown in Table 1, **13b** exhibited the strongest inhibition of NO, IL-6, and TNF- α with IC₅₀ values of 10.992 μ M, 2.294 μ M, and 12.901 μ M, respectively, followed by compound **13d** with IC₅₀ values of 19.969 μ M, 4.715 μ M, and 22.044 μ M, respectively.

Cytotoxicity of the derivatives (13b and 13d)

Subsequently, the cytotoxicity experiments of dexamethasone (DEX), **13b**, and **13d** were performed in RAW264.7 cells by using Cell Counting Kit-8 (CCK-8) assays. The results are shown in Fig. 3. During the 72 hour period, there was no discernible change in cell activity between the compound **13b** group, the control group, and the DEX group. The cell proliferation rate of compound **13d** was noticeably reduced when compared with the proliferation rates of the control group and the DEX group. These experimental results indicate that compound **13b** does

not exhibit any toxic effects on RAW264.7 cells, thus demonstrating its safety.

Structure–activity relationship of the derivatives

Based on the anti-inflammatory activity results, we summarized the structure–activity relationships of the compounds. Most of these compounds inhibited LPS-induced release of inflammatory factors from RAW264.7 cells. Notably, the compounds strongly inhibited the release of NO and IL-6, while the inhibition of TNF- α release was relatively weak. The relatively weak inhibitory effect of lead compound **12** suggests that introducing of a hydrophobic group at the amino site may enhance the activity. Branching at the α -position to the nitrogen of compound **12**, such as with a propenylcarbonyl group (**13a**), diminished IL-6 activity (IC₅₀ = 1.437 μ M) compared with compound **13b**, however, the opposite trend was observed for the TNF- α inhibition capabilities of **13a** and **13b**. Compared with **13a**, **13b** has an approximately 6-fold higher IC₅₀ for NO inhibition and an approximately 5-fold higher IC₅₀ for TNF- α . When compared with compounds **13e** and **13f**, compound **13d**, which included α -furanocarbonyl at the 5-position, demonstrated a considerable overall reduction of NO, IL-6, and TNF- α . The IC₅₀ values of compound **13d** were 19.969 μ M, 4.715 μ M, and 22.044 μ M, respectively. Among them, compound **13f** showed the most significant inhibition of IL-6 (IC₅₀ = 1.539 μ M), with poorer inhibitory vigor against NO and TNF- α . Taken together, the



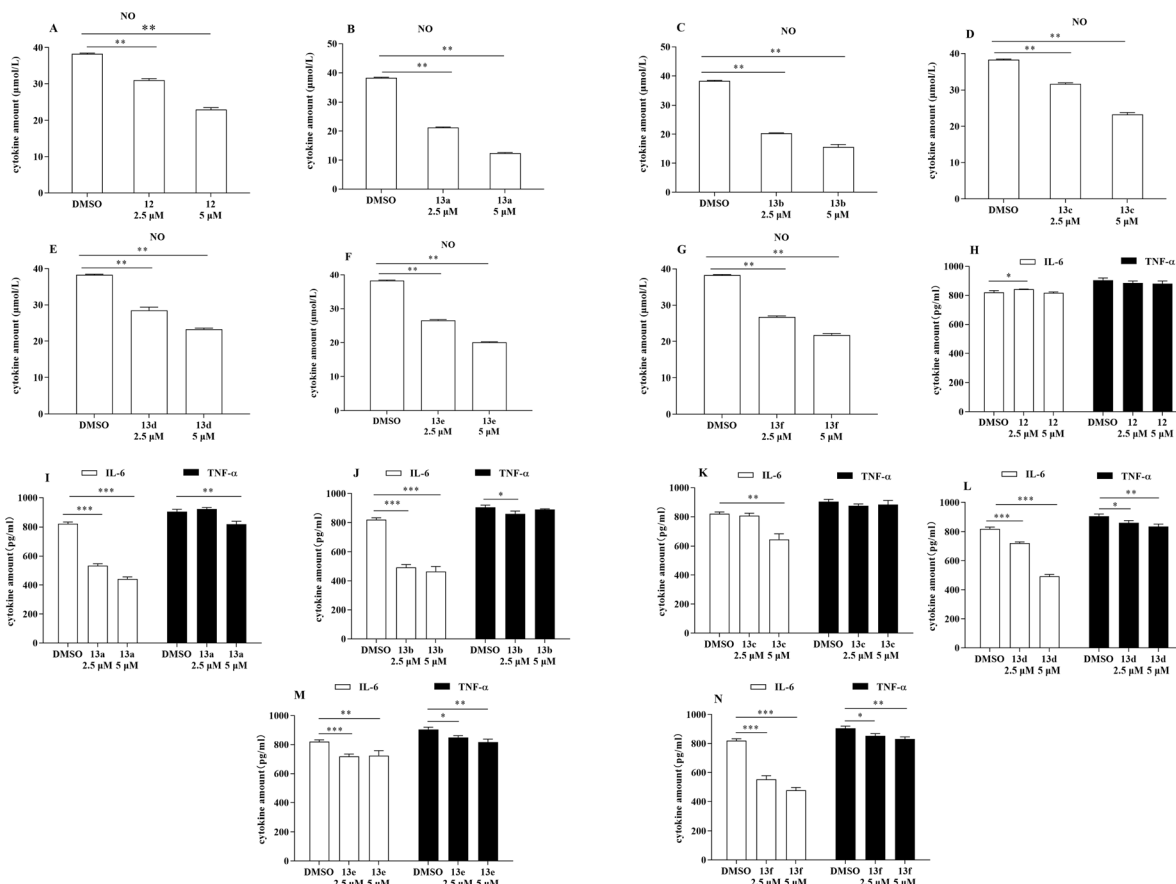


Fig. 2 Anti-inflammatory screening of compounds **12** and **13a–13f** (* $p < 0.05$, ** $p < 0.01$, *** $p < 0.001$ vs. DMSO).

Table 1 IC₅₀ of compounds **13a**, **13b**, and **13d–13f**

Compound	IC ₅₀ (μM)		
	NO	IL-6	TNF-α
DEX	21.197 ± 0.517	0.247 ± 0.073	27.796 ± 0.643
13a	61.494 ± 0.560	1.437 ± 0.351	62.835 ± 1.198
13b	10.992 ± 0.328	2.294 ± 0.791	12.901 ± 1.591
13d	19.969 ± 0.674	4.715 ± 1.995	22.044 ± 0.449
13e	22.143 ± 1.019	4.879 ± 0.112	21.795 ± 1.143
13f	36.041 ± 1.375	1.539 ± 0.515	46.777 ± 0.197

structure–activity relationships in this series are complex. Among them, compound **13b** substituted with 2-chloropropylcarbonyl was the most potent in the series with an IC₅₀ (NO) of 10.992 μM, an IC₅₀ (IL-6) of 2.294 μM and an IC₅₀ (TNF-α) of 12.901 μM. All of these findings provide new evidence for the anti-inflammatory effects of these indole-2-formamide benzimidazole[2,1-*b*]thiazole derivatives.

The promotion of ferroptosis was observed in RAW264.7 cells by compounds **13b** and **13d**

The effects of **13b** and **13d** on LPS-induced intracellular reactive ROS and MDA production in RAW264.7 cells. The results depicted in Fig. 4 and 5(A) indicate that compounds **13b**

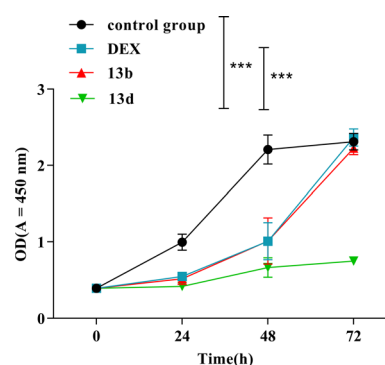


Fig. 3 Cytotoxicity evaluation of **13b** and **13d** in RAW264.7 cells (*** $P < 0.001$ vs. control group).

and **13d** had significantly affected the production of reactive oxygen species (ROS) and malondialdehyde (MDA) in LPS-induced RAW264.7 cells. The experimental findings demonstrated that both compounds significantly increased ROS and MDA levels compared with the control group, with a statistically significant increase observed. Notably, compound **13b** exerted the most pronounced effect on ROS and MDA content.

The effects of **13b** and **13d** on LPS-induced intracellular Fe²⁺ and GSH production in RAW264.7 cells. As observed in Fig. 5(B)



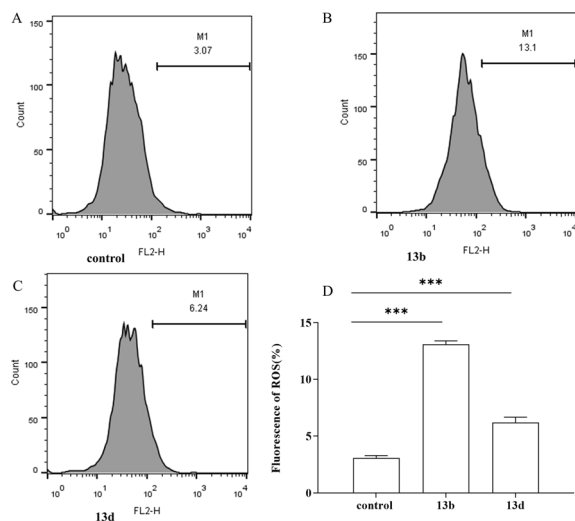


Fig. 4 The effects of **13b** and **13d** on LPS-induced intracellular ROS production in RAW264.7 cells (** $p < 0.001$ vs. control).

and (C), compounds **13b** and **13d** exhibited significant effects on the production of iron ions (Fe^{2+}) and glutathione (GSH) in RAW264.7 cells induced by LPS. The findings demonstrated that both compounds **13b** and **13d** significantly increased the levels of Fe^{2+} compared with the control group. Notably, compound **13d** had the most pronounced effect on Fe^{2+} content. Furthermore, compounds **13b** and **13d** decreased GSH content compared with the control group. Specifically, compound **13d** showed a statistically significant reduction in GSH content compared with the control group, whereas no significant difference was observed between compound **13d** and the control group.

Ferroptosis is a form of programmed cell death triggered by iron-dependent lipid peroxidation, and is characterized by the excessive accumulation of iron ions and lipid peroxides within cells.^{23,24} Previous studies have shown that ROS are essential for ferroptosis and that increasing the activity of superoxide dismutase (SOD) may efficiently reduce ROS levels *in vivo*. Intracellular iron build-up aggravates oxidative damage and promotes ferroptosis by suppressing the antioxidant system and causing the Fenton reaction, which directly produces excess ROS.^{25,26} The degree of cellular oxidative damage can be measured using MDA.^{27,28} GSH, catalyzed by glutathione peroxidase 4 (GPX4), is the most abundant intracellular antioxidant capable of scavenging ROS and inhibiting ferroptosis.^{29,30} Based on our experimental results, we observed

a significant decrease in intracellular GSH content in the treatment group. Additionally, increased levels of ROS and MDA were detected, along with intracellular Fe^{2+} accumulation, suggesting that compounds **13b** and **13d** may exert therapeutic effects through their involvement in the iron death pathway. Overall, compounds **13b** and **13d** exhibited anti-inflammatory effects by suppressing the release of inflammatory cytokines and promoting ferroptosis.

A common mechanism underlying the sepsis caused by various diseases is the entry of harmful bacteria into the body, which initiates an innate immune reaction. Macrophages are equipped with pattern-recognition receptors that recognize chemical patterns linked to infections and trigger the production of pro-inflammatory substances by immune cells. Cells respond to this stimulation by becoming inflamed, and prolonged inflammation eventually suppresses the immune system.^{31–33} Iron death, a type of regulatory cell death linked to inflammation, releases harmful molecules including high mobility group box-1 (HMGB1). Due to its immunogenic qualities, HMGB1 may intensify excessive sepsis-related inflammatory response.³⁴ Neutralizing anti-HMGB1 antibodies has been shown to be an effective way to reduce the aberrant immunological response of macrophages to systemic or local infections brought on by iron death. This suggests that HMGB1 targeting may be a therapeutic strategy for mitigating the abnormal immune response linked to iron death.³⁵ However, some studies have indicated the potential of iron-induced cell death in suppressing inflammatory responses. The steroid dexamethasone has been found to have anti-inflammatory properties and cause ferroptosis. This was accomplished by increasing the production of dipeptidase-1 by activating the glucocorticoid receptors and decreasing glutathione levels. Ferroptosis can be induced to a significant degree by dexamethasone.³⁶ Oh *et al.*³⁷ found that by blocking its effect on the NF- κ B signaling pathway in bone marrow-derived macrophages, erastin may improve the prognosis of animal models of cecal ligation and perforation (CLP) or LPS-induced septic shock. This reduced the production of inflammatory mediators. Arbiser *et al.*³⁸ utilized the ceramide analogue solenopsin to facilitate skin cell uptake and induce iron-mediated cell death for treating psoriasis, yielding remarkable outcomes and suggesting a potential positive role of iron-induced cell death in inflammation reduction. These disparities imply that the mechanism underlying iron-induced cell death may yield two distinct outcomes under different scenarios: anti-inflammatory and pro-inflammatory. Future

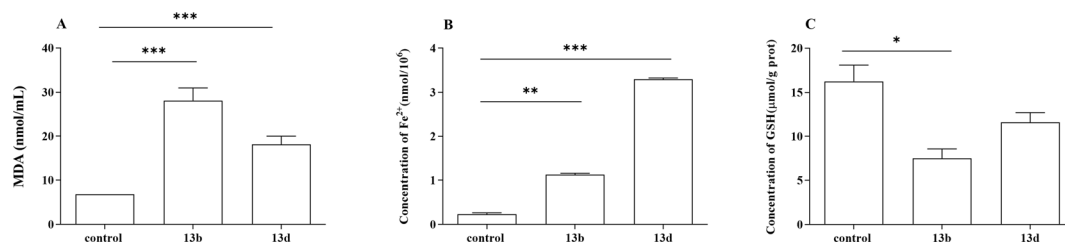


Fig. 5 The effects of **13b** and **13d** on LPS-induced intracellular MDA (A), Fe^{2+} (B) and GSH (C) production in RAW264.7 cells (* $p < 0.05$, ** $p < 0.01$, *** $p < 0.001$ vs. control).



research on septic infections should explore the conditions under which these disparities arise and how they can be harnessed to exert beneficial effects on the body.

Conclusions

The structures of a series of indole-2-formamide benzimidazole [2,1-*b*]thiazole derivatives were synthesized and characterized using hydrogen, carbon, and mass spectrometry. According to the *in vitro* cell activity results, most of the compounds demonstrated effective inhibition of the release of the inflammatory cytokines NO, IL-6, and TNF- α . Furthermore, a structure–activity relationship analysis revealed that the introduction of electron-withdrawing groups at the amino position enhanced their activity. The cytotoxicity assay showed that compound **13b** was non-toxic. Additionally, in iron death experiments, it was observed that these compounds significantly increased ROS content as well as the levels of MDA and Fe²⁺, while decreasing GSH content. This suggests their potential role in promoting the occurrence of the iron death process. In conclusion, compound **13b** not only exhibited the most efficient inhibitory effects on inflammatory factor release but also had the potential to promote iron death. Therefore, further investigation is warranted.

Experimental

Materials and characterization

All commercial chemicals and solvents were of reagent grade and were used without further purification (Changsha Junshu Biotechnology Co., Ltd, Hunan, China). TLC was performed on 0.20 mm silica gel 60 F254 plates (Qingdao Ocean Chemical Factory, Shangdong, China). Melting points were obtained using a WRS-1B melting apparatus and were uncorrected. ¹H NMR and ¹³C NMR spectra were recorded in DMSO-*d*₆ solution with a Bruker Instrument at 400 or 100 MHz, and peak positions are given in parts per million (δ) downfield from tetramethylsilane as the internal standard. *J* values are given in Hz. Mass spectra were acquired using an Agilent 6210 ESI/TOF or Agilent 6545 LC/Q-TOF mass spectrometer. All chemicals were of the highest available grade, and the purity of all synthesized compounds was >95% as determined by high performance liquid chromatography (HPLC) analysis.

General procedure for synthesis of compounds

Synthesis of 6-(3-nitrophenyl)imidazole and [2,1-*b*]thiazole-3-ethyl formate (8). At room temperature, the 2-aminothiazole-4-ethyl formate hydrochloride (4.2 g, 24.2 mmol) and the 2-bromo-3-nitroacetophenone (5.9 g, 24.2 mmol) were dissolved in 100 mL of 1,4-dioxane in a round-bottomed flask that was 250 mL in volume. A temperature of 110 °C was applied to the reaction mixture, which was then refluxed for 12 h before returning to room temperature. The reaction solution was filtered to obtain a light-yellow solid product. Next this product was washed with a small amount of anhydrous ethanol and dried to produce the desired compound, which was then

referred to as 6-(3-nitrophenyl)imidazole[2,1-*b*]thiazole-3-ethyl formate (6.5 g; compound **8**). The overall yield of this compound was 84.1%.

Synthesis of 6-(3-aminophenyl) imidazole[2,1-*b*]thiazole-3-ethyl formate (9). At room temperature, the tin(II) chloride dihydrate (3.5 g, 15.5 mmol) was carefully added to 25 mL of hydrochloric acid, and the mixture was agitated until it became completely homogeneous. After that, the 6-(3-nitrophenyl) imidazole and the [2,1-*b*]thiazole-3-ethyl formate (1.0 g, 3.2 mmol) were added to the mixture in distinct batches in a sequential manner. There was a pink suspension produced as a consequence of heating the reaction mixture to 65 °C and stirring it for 10 min. After the temperature was lowered to room temperature, stirring was continued for an additional hour before the collected solids were separated and filtered. After dissolving the solid product in water, the pH was adjusted to a value greater than seven. The aqueous solution was extracted with water and methylene chloride and the organic phase was dried simultaneously with anhydrous magnesium sulfate. This was performed before filtering and spin-drying the solvent residue. The recovered material was a yellow solid that weighed 558.4 mg (**9**), corresponding to a yield of 60.8%.

Synthesis of 6-(3-(5-nitro-1*H*-indole-2-carboxamide)phenyl) imidazole and thiazole-3-[2,1-*b*]formic acid ethyl ester (10). Under room-temperature conditions, the 5-nitro-1*H*-indole-2-formic acid (103.5 mg, 0.5 mol) and 6-(3-aminophenyl)imidazole[2,1-*b*]thiazole-3-ethyl formate (143.5 mg, 0.5 mol) were dissolved in an acceptable quantity of DMA. Subsequently, sufficient quantities of TBTU and DIPEA were added to the solution. After stirring the reaction mixture for 24 h, it was diluted with an aqueous solution of ethyl acetate and sodium bicarbonate depending on the requirements of the experiment. After filtration and sequential solid washing, the product was washed again with an aqueous solution of 1 mol L⁻¹ sodium dihydrogen phosphate. Subsequently, it was dried under vacuum to obtain a light-yellow solid compound with a weighed of 176.3 mg (**10**), which resulted in a yield of 74.2%.

Synthesis of 6-(3-(5-nitro-1-(4-(trifluoromethyl)benzyl)-1*H*-indole-2-carboxamido)phenyl)imidazole[2,1-*b*]thiazole-3-ethyl formate (11). Anhydrous acetonitrile was used to dissolve the molecule 6-[3-(5-nitro-1*H*-indole-2-formylamino)phenyl]imidazole[2,1-*b*]thiazole-3-ethyl formate (237.6 mg, 0.5 mmol). This was performed at room temperature. The progressive addition of K₂CO₃ at a concentration of 1 mmol was followed by the addition of equimolar 4-trifluoromethyl benzyl bromide at room temperature. The reaction mixture was stirred for 8 hours while being heated to 50 °C. At the end of the reaction, any remaining acetonitrile was evaporated, and then 10 mL of water was added. Ethyl acetate (20 mL \times 3) was used for the extraction process. Subsequently, the mixed organic layers were washed with 50 mL of saturated sodium chloride solution. Anhydrous magnesium sulfate was used to dry the substance, and filtering was performed at a decreased pressure. The concentrated crude residue was purified by silica gel column chromatography using an eluent that consisting of a combination of ethyl acetate and petroleum ether at a ratio of 1 : 5. This resulted in the production of 222.2 mg (**11**), corresponding to a yield of 70.2%.



Synthesis of 6-(3-(5-amino-4-chloro-1-(4-(trifluoromethyl)benzyl)-1H-indole-2-carboxamido)phenyl)imidazole[2,1-b]thiazole-3-ethyl formate (12). In a round bottom flask, 6-(3-(5-nitro-1-(4-(trifluoromethyl)benzyl)-1H-indole-2-formamido)phenyl)imidazole[2,1-b]thiazole-3-ethyl formate (663.1 mg, 1 mmol) was added, followed by 100 mL of anhydrous ethanol. To perform the reflux reaction at room temperature for 3 h, 10 mL of strong hydrochloric acid and tin(II) chloride dihydrate were added. Subsequently, a solution of 1 M sodium hydroxide was added to the mixture which was kept in an ice bath. This was done to reduce the pH to approximately 7. The filter cake was washed with ethanol and ethyl acetate was used to extract the mother liquor after the washing. The organic layer was rinsed, dried, and spun-dried in saturated salt water once the process was completed. Finally, a white chemical (12), which weight of 286.65 mg, was successfully isolated using column chromatography, resulting in a yield of 45%.

General procedure A for the preparation of indole-2-formamide benzimidazol[2,1-b]thiazole derivatives (13a–13f)

Following the addition of 6 mL of DMA and 0.75 mmol of an acyl chloride derivative, compound 12 was mixed into a flask with a round bottom while the temperature was kept at room temperature. Twenty-four hours were spent stirring the reaction mixture at room temperature, while TLC was used to check its progress. The reaction was stopped by adding 20 mL of a saturated sodium bicarbonate solution after the starting ingredient had completely passed away. The final product, 13a–13f, using ethyl acetate (20 mL × 3), combined it with the organic layer, dried it with anhydrous magnesium sulfate, and then separating it using column chromatography. The yield of the product ranged from 56 to 82%.

Ethyl 6-(3-(5-amino-4-chloro-1-(4-(trifluoromethyl)benzyl)-1H-indole-2-carboxamido)phenyl)imidazole[2,1-b]thiazole-3-carboxylate (12). Yield: 75.2%; mp 116.4–118.1 °C; white powder. ¹H NMR (400 MHz, DMSO-*d*₆) δ 10.40 (s, 1H), 8.41 (s, 1H), 8.36 (t, *J* = 1.7 Hz, 1H), 8.27 (s, 1H), 7.66 (ddd, *J* = 19.5, 10.2, 8.1 Hz, 4H), 7.42 (s, 1H), 7.37 (t, *J* = 7.9 Hz, 1H), 7.28 (d, *J* = 8.9 Hz, 1H), 7.25 (d, *J* = 8.1 Hz, 2H), 6.89 (d, *J* = 8.8 Hz, 1H), 5.94 (s, 2H), 5.05 (s, 2H), 4.42 (q, *J* = 7.1 Hz, 2H), 1.38 (t, *J* = 7.1 Hz, 3H). ¹³C NMR (101 MHz, DMSO-*d*₆) δ 160.49, 157.98, 148.73, 147.04, 144.20, 139.79, 139.32, 134.65, 132.82, 131.45, 129.45, 128.24, 127.92, 127.45, 126.05, 125.84, 125.71, 125.07, 123.44, 123.35, 120.79, 119.66, 117.29, 116.67, 110.99, 110.78, 106.93, 104.12, 62.30, 47.51, 14.53. HRMS: (ESI, *m/z*): calcd for C₃₁H₂₃ClF₃N₅O₃S ([M + H]⁺), 637.12; found, 638.1241.

Ethyl 6-(3-(5-acrylamido-4-chloro-1-(4-(trifluoromethyl)benzyl)-1H-indole-2-carboxamido)phenyl)imidazole[2,1-b]thiazole-3-carboxylate (13a). Yield: 68.2%; mp 183.5–186.3 °C, white powder. ¹H NMR (400 MHz, DMSO-*d*₆) δ 10.55 (s, 1H), 9.87 (s, 1H), 8.42 (s, 1H), 8.37 (s, 1H), 8.27 (s, 1H), 7.72–7.63 (m, 5H), 7.57–7.48 (m, 2H), 7.39 (t, *J* = 7.9 Hz, 1H), 7.29 (d, *J* = 8.1 Hz, 2H), 6.59 (dd, *J* = 17.0, 10.2 Hz, 1H), 6.28 (dd, *J* = 17.1, 1.9 Hz, 1H), 6.04 (s, 2H), 5.81–5.76 (m, 1H), 4.43 (q, *J* = 7.1 Hz, 2H), 1.38 (t, *J* = 7.1 Hz, 3H). ¹³C NMR (101 MHz, DMSO-*d*₆) δ 164.14, 160.16, 157.98, 148.75, 146.98, 143.71, 139.59, 137.08, 134.71,

132.84, 131.92, 129.52, 128.46, 127.52, 127.52, 127.43, 126.02, 125.98, 125.94, 125.91, 125.17, 125.10, 124.72, 123.45, 121.02, 120.76, 119.75, 117.38, 110.83, 110.48, 105.67, 79.65, 62.31, 14.53. HRMS: (ESI, *m/z*): calcd for C₃₄H₂₅ClF₃N₅O₄S ([M + H]⁺), 691.13; found, 692.1346.

Ethyl 6-(3-(4-chloro-5-(2-chloropropanamido)-1-(4-(trifluoromethyl)benzyl)-1H-indole-2-carboxamido)phenyl)imidazole[2,1-b]thiazole-3-carboxylate (13b). Yield: 70.3%; mp 146.4–148.6 °C; light red powder. ¹H NMR (400 MHz, DMSO-*d*₆) δ 10.56 (s, 1H), 10.04 (s, 1H), 8.42 (s, 1H), 8.38 (s, 1H), 8.26 (s, 1H), 7.75–7.63 (m, 5H), 7.57 (d, *J* = 8.9 Hz, 1H), 7.44–7.36 (m, 2H), 7.30 (d, *J* = 8.0 Hz, 2H), 6.05 (s, 2H), 4.85 (q, *J* = 6.7 Hz, 1H), 4.42 (q, *J* = 7.1 Hz, 2H), 1.68 (d, *J* = 6.7 Hz, 3H), 1.38 (t, *J* = 7.1 Hz, 3H). ¹³C NMR (101 MHz, DMSO-*d*₆) δ 168.57, 160.12, 157.96, 148.74, 146.99, 143.68, 139.58, 137.32, 134.71, 132.99, 129.49, 127.82, 127.48, 127.48, 125.96, 125.92, 125.88, 125.24, 125.04, 125.04, 124.62, 123.42, 121.51, 121.02, 119.74, 117.40, 110.80, 110.61, 105.69, 79.64, 62.28, 54.80, 21.91, 14.50. HRMS: (ESI, *m/z*): calcd for C₃₄H₂₆Cl₂F₃N₅O₄S ([M + H]⁺), 727.10; found, 728.1115.

Ethyl 6-(3-(4-chloro-5-propionamido)-1-(4-(trifluoromethyl)benzyl)-1H-indole-2-carboxamido)phenyl)imidazole[2,1-b]thiazole-3-carboxylate (13c). Yield: 56.7%; mp 175.2–178.1 °C, earthy yellow powder. ¹H NMR (400 MHz, DMSO-*d*₆) δ 10.54 (s, 1H), 9.57 (s, 1H), 8.42 (s, 1H), 8.37 (s, 1H), 8.27 (s, 1H), 7.73–7.63 (m, 5H), 7.53 (d, *J* = 8.9 Hz, 1H), 7.40 (dd, *J* = 8.3, 6.2 Hz, 2H), 7.29 (d, *J* = 8.1 Hz, 2H), 6.04 (s, 2H), 4.42 (q, *J* = 7.1 Hz, 2H), 2.39 (q, *J* = 7.5 Hz, 2H), 1.38 (t, *J* = 7.1 Hz, 3H), 1.13 (t, *J* = 7.5 Hz, 3H). ¹³C NMR (101 MHz, DMSO-*d*₆) δ 172.82, 160.18, 157.96, 148.74, 146.98, 143.75, 139.61, 137.01, 134.70, 132.71, 129.50, 129.06, 128.87, 127.48, 127.48, 125.99, 125.96, 125.92, 125.89, 125.17, 125.08, 125.08, 123.43, 120.99, 119.73, 117.37, 110.81, 110.35, 105.66, 79.65, 62.29, 29.24, 14.52, 10.34. HRMS: (ESI, *m/z*): calcd for C₃₄H₂₇ClF₃N₅O₄S ([M + H]⁺), 693.14; found, 694.1510.

Ethyl 6-(3-(4-chloro-5-(furan-2-carboxamido)-1-(4-(trifluoromethyl)benzyl)-1H-indole-2-carboxamido)phenyl)imidazole[2,1-b]thiazole-3-carboxylate (13d). Yield: 62.5%; mp 291.5–294.6 °C, white powder. ¹H NMR (400 MHz, DMSO-*d*₆) δ 10.56 (s, 1H), 10.04 (s, 1H), 8.43 (s, 1H), 8.37 (s, 1H), 8.27 (s, 1H), 7.96 (s, 1H), 7.75–7.54 (m, 6H), 7.44–7.26 (m, 5H), 6.72 (dd, *J* = 3.4, 1.7 Hz, 1H), 6.06 (s, 2H), 4.42 (q, *J* = 7.1 Hz, 2H), 1.38 (t, *J* = 7.1 Hz, 3H). ¹³C NMR (101 MHz, DMSO-*d*₆) δ 160.14, 157.98, 157.14, 148.75, 147.89, 146.97, 146.19, 143.72, 139.58, 137.51, 134.71, 132.93, 129.53, 129.07, 128.39, 128.08, 127.84, 127.50, 125.99, 125.71, 125.30, 125.11, 123.44, 123.32, 122.85, 121.02, 119.75, 117.39, 115.19, 112.61, 110.84, 110.58, 105.73, 79.65, 62.31, 14.53. HRMS: (ESI, *m/z*): calcd for C₃₆H₂₅ClF₃N₅O₅S ([M + H]⁺), 731.12; found, 732.1298.

Ethyl 6-(3-(5-benzamido-4-chloro-1-(4-(trifluoromethyl)benzyl)-1H-indole-2-carboxamido)phenyl)imidazole[2,1-b]thiazole-3-carboxylate (13e). Yield: 82.1%; mp 251.1–253.4 °C, yellow powder. ¹H NMR (400 MHz, DMSO-*d*₆) δ 10.56 (s, 1H), 10.16 (s, 1H), 8.43 (s, 1H), 8.37 (s, 1H), 8.26 (s, 1H), 8.04 (d, *J* = 7.3 Hz, 2H), 7.71 (d, *J* = 7.5 Hz, 2H), 7.67 (d, *J* = 5.1 Hz, 2H), 7.63 (d, *J* = 8.1 Hz, 1H), 7.60 (s, 1H), 7.58 (d, *J* = 2.3 Hz, 2H), 7.56 (s, 1H), 7.44–7.36 (m, 2H), 7.31 (d, *J* = 8.1 Hz, 2H), 6.07 (s, 2H), 4.43 (q, *J* = 7.1 Hz, 2H), 1.38 (t, *J* = 7.1 Hz, 3H). ¹³C NMR (101 MHz,



DMSO- d_6) δ 166.16, 160.18, 157.97, 148.76, 146.99, 143.74, 139.59, 137.56, 134.71, 134.61, 132.90, 132.20, 129.52, 128.94, 128.94, 128.73, 128.41, 128.15, 128.15, 127.49, 127.49, 126.08, 126.02, 125.98, 125.95, 125.34, 125.07, 123.45, 123.12, 121.03, 119.78, 117.42, 110.83, 110.53, 105.77, 79.64, 62.31, 14.52. HRMS: (ESI, m/z): calcd for $C_{38}H_{27}ClF_3N_5O_4S$ ($[M + H]^+$), 741.14; found, 742.1506.

Ethyl 6-(3-(4-chloro-5-(4-fluorobenzamido)-1-(4-(trifluoromethyl)benzyl)-1H-indole-2-carboxamido)phenyl)imidazole[2,1-b]thiazole-3-carboxylate (13f). Yield: 75.8%; mp 155.3–158.5 °C; orange powder. 1H NMR (400 MHz, DMSO- d_6) δ 10.56 (s, 1H), 10.20 (s, 1H), 8.43 (s, 1H), 8.37 (s, 1H), 8.27 (s, 1H), 8.11 (dd, J = 8.6, 5.6 Hz, 2H), 7.72–7.63 (m, 5H), 7.59 (d, J = 8.9 Hz, 1H), 7.39 (t, J = 8.1 Hz, 3H), 7.30 (d, J = 8.1 Hz, 3H), 6.07 (s, 2H), 4.43 (q, J = 7.1 Hz, 2H), 1.38 (t, J = 7.1 Hz, 3H). ^{13}C NMR (101 MHz, DMSO) δ 165.09, 163.41, 160.16, 157.98, 148.76, 146.99, 143.72, 139.59, 137.59, 134.71, 132.92, 131.08, 131.05, 130.92, 130.83, 129.52, 128.61, 127.50, 127.50, 126.08, 126.02, 125.99, 125.95, 125.33, 125.09, 123.45, 123.17, 121.03, 119.77, 117.42, 116.01, 115.80, 115.80, 110.83, 110.56, 105.76, 62.30, 14.53. HRMS: (ESI, m/z): calcd for $C_{38}H_{26}ClF_4N_5O_4S$ ($[M + H]^+$), 759.13; found, 760.1409.

The characterization 1H NMR, ^{13}C NMR, HR-ESI-MS data of target compounds are shown in the ESI.†

Biological evaluation

Cell culture and reagents. Lipopolysaccharide (LPS, *Escherichia coli* O111:B4) was obtained from Sigma-Aldrich LLC. TNF- α and IL-6 ELISA kits were obtained from Boster Biological Technology Co., Ltd. Nitric Oxide (NO) assay kits were obtained from 3-Bio Technology Co., Ltd (Shanghai, China). Malondialdehyde (MDA) reactive oxygen species (ROS), and Micro Reduced Glutathione Assay Kits were obtained from Nanjing Jiancheng Bioengineering Institute (Nanjing, China). Cell Ferrous Iron Colorimetric Assay Kit was obtained from Elabscience Biotechnology Co., Ltd (Wuhan, China).

The RAW264.7 cells were cultured in a humidified incubator at 37 °C with 5% CO₂. The culture medium used was Dulbecco's Modified Eagle's Medium (DMEM) supplemented with 10% FBS (Hyclone, Logan, UT, USA), 100 U mL⁻¹ of penicillin, and 100 mg mL⁻¹ of streptomycin.

The organization and intervention of cells

The cells were at a density of 4×10^5 cells in milliliter for RAW264.7 cells that were in the logarithmic growth phase in 96-well plates and incubated for 24 h prior to drug administration. In the indomethacin-treated and experimental groups, macrophages were incubated for 30 min, followed by stimulation with LPS (0.5 mg L⁻¹), and then for an additional 24 h.

The impact of target compounds on the level of NO released from LPS-induced RAW264.7 cells

The Griess technique was used in order to determine the amount of nitric oxide (NO) that was present in the supernatant of RAW264.7 cells that had been stimulated by LPS. The NO

content of each sample was determined by referring to an NaNO₂ standard curve.

The impact of target compounds on the production of IL-6 and TNF- α cytokines LPS-induced RAW264.7 cells

After treatment of RAW264.7 cells, IL-6 and TNF- α concentration in culture medium was determined with commercial ELISA assay kits according to its manufacturer's instructions. The absorbance was measured using a microplate reader at 450 nm, and the concentrations were calculated using a standard curve.

Cytotoxicity experiments of 13b and 13d

The cytotoxicity of compounds **13b** and **13d** were evaluated in RAW264.7 cells. Cell viability was determined using the CCK-8 assay. Cells (1×10^4 cells per well) in 96-well plates were treated with different concentrations of molecule for 24, 48 and 72 h. Then, removed the culture medium from the wells and added 100 μ L of the CCK-8 working solution (10% CCK-8 reagent in the culture medium), followed by incubation at 37 °C in a 5% CO₂ humidified incubator. The absorbance of each well was measured at 450 nm using a microplate reader at the following concentrations: (1) control group: normal medium; (2) dexamethasone (DEX): 27.964 μ M; (3) compound **13b**: 12.326 μ M (4) compound **13d**: 23.684 μ M.

Measurement of indicators related to iron death

After treatment of RAW264.7 cells, ROS, MDA, GSH and Fe²⁺ concentrations in the culture medium were determined using commercial ELISA assay kits according to the manufacturer's instructions (compounds **13a** and **13b**: 10 μ M).

Statistical analysis

Statistical analyses were analyzed by GraphPad Prism 9.5.1, and expressed as mean \pm standard (SD). Statistical data were considered to be statistically significant if p -values less than 0.05.

Author contributions

Yu-Cai Jiang and Hai-Feng Lin conceived the study and supervised the study. Hai-Feng Lin, Yu-Cai Jiang, Zhi-Wei Chen and Lin-Lin Zheng performed the experiments. Hai-Feng Lin, Yu-Cai Jiang and Zhi-Wei Chen analyzed data. Yu-Cai Jiang wrote the manuscript. Hai-Feng Lin, Yu-Cai Jiang, Zhi-Wei Chen and Lin-Lin Zheng review the manuscript and discussion of results. All the authors have read and approved the final version of the manuscript.

Conflicts of interest

The authors declare that they have no known competing financial interests or personal relationships that could have appeared to influence the work reported in this study.



Acknowledgements

This study was supported by the Natural Science Foundation of Fujian Province of China (2021J011376), Educational Commission of Fujian Province of China (JAT200512), Educational Commission of Fujian Province of China (JAT210398), and the Scientific Research Project of Putian University (2021031).

Notes and references

- 1 Z. Ju, Z. Shang, T. Mahmud, J. Fang, Y. Liu, Q. Pan, X. Lin and F. Chen, *J. Nat. Prod.*, 2023, **86**, 958–965.
- 2 L. Z. Chen, L. Yao, M. M. Jiao, J. B. Shi, Y. Tan, B. F. Ruan and X. H. Liu, *Eur. J. Med. Chem.*, 2019, **175**, 114–128.
- 3 S. Lv, M. Han, R. Yi, S. Kwon, C. Dai and R. Wang, *Int. J. Clin. Pract.*, 2014, **68**, 520–528.
- 4 L. Song, G. Li, W. Guan, Z. Zeng, Y. Ou, T. Zhao, J. Li, D. He, X. Fang, Y. Zhang, J. Q. Wu, R. Tong and H. Yao, *Biomed. Pharmacother.*, 2023, **166**, 115412.
- 5 M. Naffaa, B. F. Makhoul, A. Tobia, M. Kaplan, D. Aronson, W. Saliba and Z. S. Azzam, *Am. J. Emerg. Med.*, 2013, **31**, 1361–1364.
- 6 F. Imam, N. O. Al-Harbi, M. M. Al-Harbi, M. A. Ansari, K. M. Zoheir, M. Iqbal, M. K. Anwer, A. R. Al Hoshani, S. M. Attia and S. F. Ahmad, *Pharmacol. Res.*, 2015, **102**, 1–11.
- 7 W. Albrecht, A. Unger, S. M. Bauer and S. A. Laufer, *J. Med. Chem.*, 2017, **60**, 5290–5305.
- 8 S. S. Zhang, Q. W. Tan and L. P. Guan, *Mini-Rev. Med. Chem.*, 2021, **21**, 2261–2275.
- 9 O. Soyer Can, S. Ünlü, H. Ocak, E. Ç. Çöldür, H. Sipahi and B. Bilgin Eran, *J. Iran. Chem. Soc.*, 2021, **19**, 579–587.
- 10 B. Karaman and N. Ulusoy Güzel demirci, *Med. Chem. Res.*, 2016, **25**, 2471–2484.
- 11 F. Centofanti, A. Buono, M. Verboni, C. Tomino, S. Lucarini, A. Duranti, P. P. Pandolfi and G. Novelli, *Pharmaceuticals*, 2023, **16**, 240.
- 12 M. A. Salem, A. Ragab, A. A. Askar, A. El-Khalafawy and A. H. Makhoulouf, *Eur. J. Med. Chem.*, 2020, **188**, 111977.
- 13 M. A. Syed, P. R. Yiragamreddy and K. B. Chandrasekhar, *Immunobiology*, 2017, **27**(4), 329–338.
- 14 S. Hou, X. Yang, Y. Tong, Y. Yang, Q. Chen, B. Wan, R. Wei, Y. Wang, Y. Zhang, B. Kong, J. Huang, Y. Chen, T. Lu, Q. Hu and D. Du, *Eur. J. Med. Chem.*, 2021, **211**, 113114.
- 15 N. S. Shetty, I. A. M. Khazi and C.-J. Ahn, *Bull. Korean Chem. Soc.*, 2010, **31**, 2337–2340.
- 16 E. D. Dincel, E. Gursoy, T. Yilmaz-Ozden and N. Ulusoy-Guzeldemirci, *Bioorg. Chem.*, 2020, **103**, 104220.
- 17 P. V. Thanikachalam, R. K. Maurya, V. Garg and V. Monga, *Eur. J. Med. Chem.*, 2019, **183**, 111680.
- 18 Y. Huang, B. Zhang, J. Li, H. Liu, Y. Zhang, Z. Yang and W. Liu, *Eur. J. Med. Chem.*, 2019, **180**, 41–50.
- 19 M. B. Tehrani, S. Emami, M. Asadi, M. Saeedi, M. Mirzahekmati, S. M. Ebrahimi, M. Mahdavi, H. Nadri, A. Moradi, F. H. Moghadam, S. Farzipour, M. Vosooghi, A. Foroumadi and A. Shafiee, *Eur. J. Med. Chem.*, 2014, **87**, 759–764.
- 20 Z. Liu, L. Tang, H. Zhu, T. Xu, C. Qiu, S. Zheng, Y. Gu, J. Feng, Y. Zhang and G. Liang, *J. Med. Chem.*, 2016, **59**, 4637–4650.
- 21 M. H. Guo, P. Wen, Y. Xiao, W. S. Ji, X. L. Zhou, F. Gao and L. H. Shan, *Fitoterapia*, 2023, **168**, 105536.
- 22 S. Wang, G. Dong and C. Sheng, *Chem. Rev.*, 2019, **119**, 4180–4220.
- 23 Q. Song, S. Peng, F. Che and X. Zhu, *J. Pharmacol. Sci.*, 2022, **148**, 300–306.
- 24 X. Jiang, B. R. Stockwell and M. Conrad, *Nat. Rev. Mol. Cell Biol.*, 2021, **22**, 266–282.
- 25 X. Chen, R. Kang, G. Kroemer and D. Tang, *Nat. Rev. Clin. Oncol.*, 2021, **18**, 280–296.
- 26 H. Wang, P. An, E. Xie, Q. Wu, X. Fang, H. Gao, Z. Zhang, Y. Li, X. Wang, J. Zhang, G. Li, L. Yang, W. Liu, J. Min and F. Wang, *Hepatology*, 2017, **66**, 449–465.
- 27 J. Du, Y. Zhou, Y. Li, J. Xia, Y. Chen, S. Chen, X. Wang, W. Sun, T. Wang, X. Ren, X. Wang, Y. An, K. Lu, W. Hu, S. Huang, J. Li, X. Tong and Y. Wang, *Redox Biol.*, 2020, **32**, 101483.
- 28 L. Li, S. Sun, L. Tan, Y. Wang, L. Wang, Z. Zhang and L. Zhang, *Nano Lett.*, 2019, **19**, 7781–7792.
- 29 J. Cao, X. Chen, L. Jiang, B. Lu, M. Yuan, D. Zhu, H. Zhu, Q. He, B. Yang and M. Ying, *Nat. Commun.*, 2020, **11**, 1251.
- 30 Z. Tang, Y. Ju, X. Dai, N. Ni, Y. Liu, D. Zhang, H. Gao, H. Sun, J. Zhang and P. Gu, *Redox Biol.*, 2021, **43**, 101971.
- 31 S. L. Raymond, D. C. Holden, J. C. Mira, J. A. Stortz, T. J. Loftus, A. M. Mohr, L. L. Moldawer, F. A. Moore, S. D. Larson and P. A. Efron, *Biochim. Biophys. Acta, Mol. Basis Dis.*, 2017, **1863**, 2564–2573.
- 32 O. Takeuchi and S. Akira, *Cell*, 2010, **140**, 805–820.
- 33 R. V. D'Elia, K. Harrison, P. C. Oyston, R. A. Lukaszewski and G. C. Clark, *Clin. Vaccine Immunol.*, 2013, **20**, 319–327.
- 34 G. H. Son, Y. Kim, J. J. Lee, K. Y. Lee, H. Ham, J. E. Song, S. T. Park and Y. H. Kim, *Sci. Rep.*, 2019, **9**, 19746.
- 35 Q. Wen, J. Liu, R. Kang, B. Zhou and D. Tang, *Biochem. Biophys. Res. Commun.*, 2019, **510**, 278–283.
- 36 A. von Mässenhausen, N. Zamora Gonzalez, F. Maremonti, A. Belavgeni, W. Tonnus, C. Meyer, K. Beer, M. T. Hannani, A. Lau, M. Peitzsch, P. Hoppenz, S. Locke, T. Chavakis, R. Kramann, D. A. Muruve, C. Hugo, S. R. Bornstein and A. Linkermann, *Sci. Adv.*, 2022, **8**, eabl8920.
- 37 B. M. Oh, S. J. Lee, G. L. Park, Y. S. Hwang, J. Lim, E. S. Park, K. H. Lee, B. Y. Kim, Y. T. Kwon, H. J. Cho and H. G. Lee, *J. Clin. Med.*, 2019, **8**, 2210.
- 38 J. L. Arbiser, M. Y. Bonner, N. Ward, J. Elsey and S. Rao, *Biochim. Biophys. Acta, Gen. Subj.*, 2018, **1862**, 2518–2527.

